IEEE Access
Multidisciplinary ⋮ Rapid Review ⋮ Open Access Journal

Received March 13, 2022, accepted April 3, 2022, date of publication April 7, 2022, date of current version April 18, 2022.

Digital Object Identifier 10.1109/ACCESS.2022.3165664

Two-Stage Converter Standalone PV-Battery System Based on VSG Control

HASHIM HASABELRASUL[1], ZHENJIANG CAI[1], LEI SUN[1], XUESONG SUO[1], AND IMAD MATRAJI[2]

[1]College of Mechanical and Electrical Engineering, Hebei Agricultural University, Baoding 071001, China
[2]Great Wall Motors, FTXT Energy Technology Company Ltd., Baoding 071000, China

Corresponding author: Zhenjiang Cai (czj65@163.com)

This work was supported in part by the Postdoctoral Program of Hebei Agricultural University, Science and Technology Support Program of Baoding under Grant 18ZG011; in part by the Key Research and Development Project of Hebei Province under Grant 19227401D and Grant 19227206D; in part by the Hebei Province to Introduce Overseas Students under Project C201834 and Project C201835; and in part by the Hebei University Science and Technology Research Project under Grant QN2018081. The work of Hashim Hasabelrasul was supported by the Postdoctoral Program of Hebei Agricultural University.

ABSTRACT Standalone solar PV systems have emerged as potential alternatives to electricity problems in areas where a grid is unavailable. Obtaining full power from a photoelectric system, DC-DC inverter, DC-AC converter, and control system presents great difficulties when building these devices. A standalone two-stage approach is introduced in this work with a boost converter followed by an inverter and a battery with a bidirectional converter. In this paper, a novel virtual synchronous generator (VSG) controller is designed and implemented to adjust the inverter output. The VSG element and the maximum power point tracking (MPPT) used in this study serve the following purposes: to adjust the inverter output and to realize the maximum power of the PV scheme. The new control strategy design was evaluated and validated using extensive MATLAB simulations under different scenarios, including load variations. The system output was evaluated using extensive MATLAB simulations. A hands-on experiment was conducted for the VSG using console testing. Due to the lack of laboratory equipment, we could not experiment with the entire system.

INDEX TERMS MPPT, DC-DC boost converter, PV array, virtual synchronous generator, two-stage converter, DC-AC inverter, battery.

I. INTRODUCTION

PV systems are increasingly being used as distributed generators worldwide because they are environmentally sustainable and clean. The price of PV panels has dropped significantly, and they typically have DC power, which is not always stable. Therefore, before the PV signals can be fed to the output load or linked to the grid power, they require DC-DC or DC-AC conversions. However, since PV power is unstable, standalone PV units need an energy power storage component, usually implemented by a battery bank [1]–[8].

PV supplies change over time because of the source and condition's variable nature under the load or grid specification demand. A single and a two-stage process are two methods used to integrate the solar energy with the load or grid [9]–[11]. The first method is made up of inverters that convert DC to AC according to the load's demand. In the second one, however, the DC voltage supplied by PV cells is first increased and then inverted into AC as needed [12], [13].

Recently, studies on two-stage grid converter structures of standalone applications have been limited. In [14], a two-stage single-phase PV system designed to operate in a standalone configuration without batteries was presented. The authors concluded that the device could adequately provide stand-alone power without the use of batteries. Thus, the system costs and maintenance can be reduced if the system is designed practically. Article [15] introduced a proportional-integral (PI) design to control a two-stage standalone system. The control goals were achieved with satisfaction and success, as per the obtained results.

However, these works do not mention how a VSG control can operate under a two-stage converter. This paper focused on a two-stage converter operating in a standalone mode with a battery based on the VSG control system application.

The associate editor coordinating the review of this manuscript and approving it for publication was Yijie Wang.

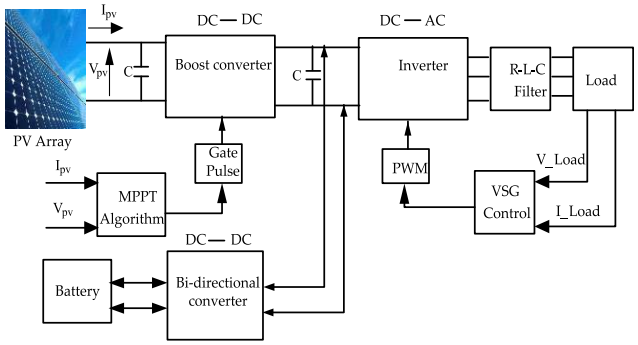

FIGURE 1. Schematic circuit diagram for a two-stage converter.

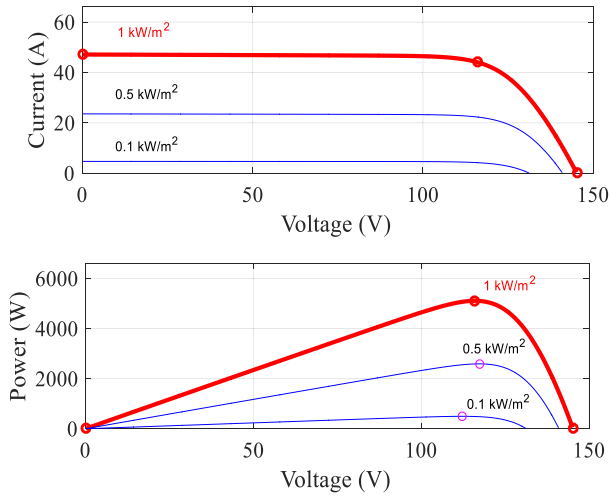

FIGURE 2. Characteristic curves of a PV array.

II. PROPOSED CIRCUIT

A. MAIN CIRCUIT

Fig. 1 depicts a schematic diagram of a two-stage converter. A DC-DC, DC-AC, and a storage unit through a bidirectional converter via the PV power source to supply the load are observed. The system also contains the control system of the two stages.

B. THE PV ARRAY

Solar PV units are linked in parallel and series combinations to provide higher power production and create solar PV arrays. This article's PV array has six parallel and four series panels with a combined input capacity of 5 kW. The solar module parameters are shown in Table 1. Fig. 2 presents the solar panel characteristic curves.

C. DESIGN OF THE CONVERTER DC-DC

A boost converter is employed to achieve the required voltage. Fig. 3 presents the design of the frame structure of the DC-DC stage.

The design specifications are defined as follows:

TABLE 1. PV unit parameters.

Quantity	Value
Module power	213.15 W
Module voltage	29 V
Module current	7.35 A
Open-circuit module voltage	36.3 V
The short-circuit module current	7.84 A

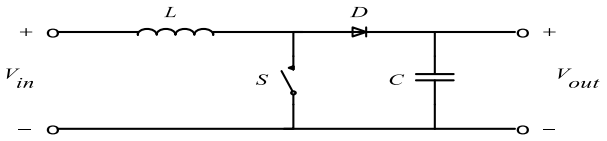

FIGURE 3. Circuit diagram for the boost converter.

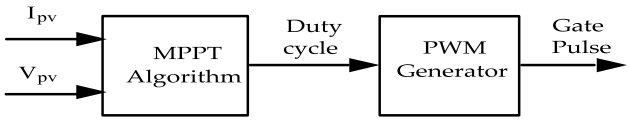

FIGURE 4. MPPT I/O block diagram.

Input voltage V_{in} = 100 to 150 V, switching frequency f_{sw} = 5 kHz, output voltage V_{out} = 500 Vd_c, rated power P = 5 kW, current ripple $\Delta I = 5\%$, voltage ripple $\Delta V = 1\%$. Then, I_{in} = 33 to 50 A and ΔI = 1.65 to 2.5. The inductance capacitance is calculated as:

$$L = \frac{V_{in}(V_{out} - V_{in})}{fsw^{*}\Delta I^{*}V_{out}} = 6.4 \text{ to } 12.7\text{mH} \quad (1)$$

$$C = \frac{I_{out}(V_{out} - V_{in})}{fsw^{*}\Delta V^{*}V_{out}} = 280 \text{ to } 320\mu\text{F} \quad (2)$$

III. THE CONTROL SYSTEM

A. MPPT ALGORITHM CONTROL

The values of PV panel calculations based on PV current and voltage are described in the block diagram shown in Fig. 4. Through this process, converter gate pulses are obtained.

Fig. 5 presents the duty-cycle controlled flow chart MPPT algorithm used to verify the PV unit's power on maximum point. The voltage state of the power is determined by multiplying the PV panel current and voltage with the previous one in the duty-cycle control approach. It checks the voltage sampling value of the voltage with the last value in the same way and regulates the duty to obey the power on the maximum point based on the result of the matching power.

B. VSG METHOD

Fig. 6 shows an inverter block diagram with a control based on the VSG, which consists of the power load and control circuit. The input of this stage is the current and voltage of the load, and its output is the PWM signal used for switching the inverter.

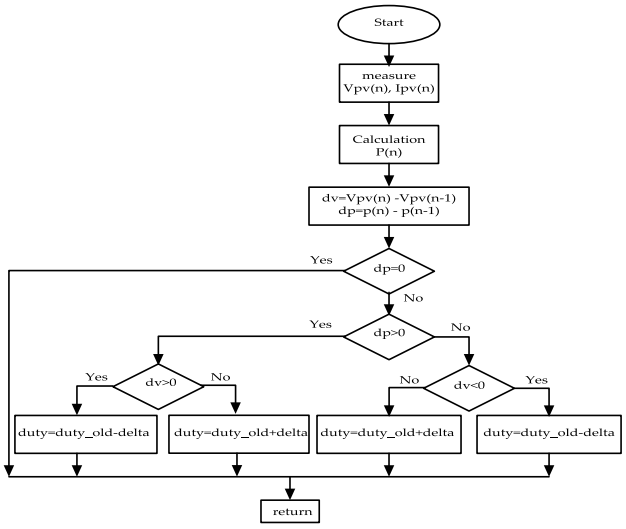

FIGURE 5. Duty cycle control algorithm.

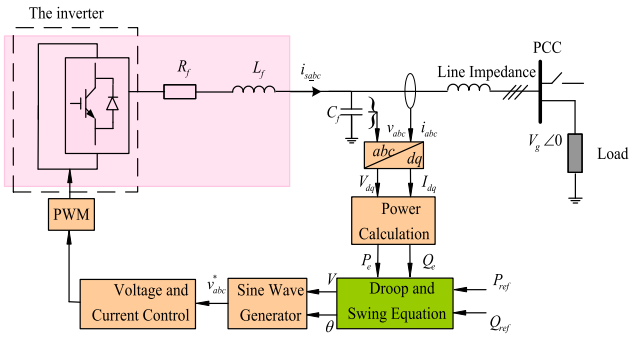

FIGURE 6. Structure of VSG control.

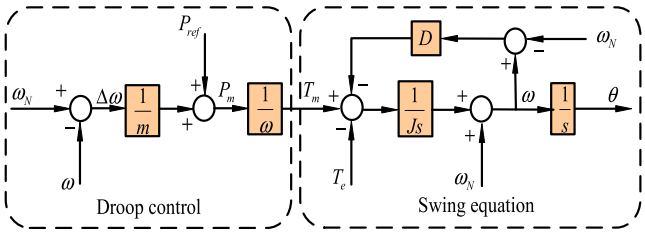

FIGURE 7. The active power loop of VSG.

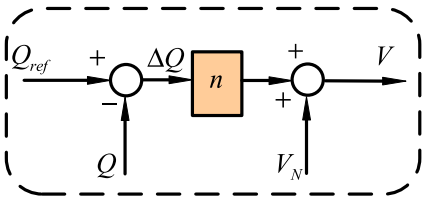

FIGURE 8. The reactive power-voltage droop control loop of VSG.

The VSG active and reactive power loops are described in Fig. 7 and Fig. 8, respectively.

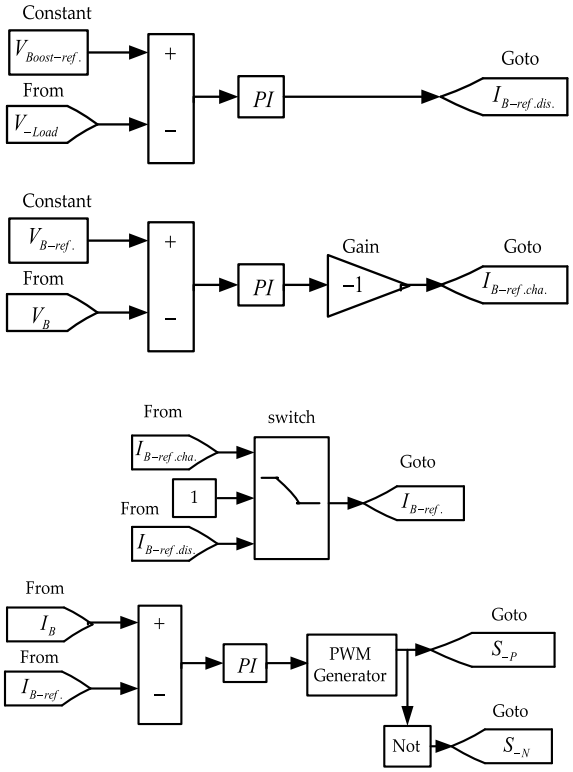

FIGURE 9. MATLAB simulation battery charge and discharge control.

TABLE 2. The battery parameters.

Quantity	Value
Nominal voltage	220 V
Rated capacity (Ah)	100
Initial SOC %	50
Fully charged voltage	256 V

The droop equations are expressed as:

$$\omega = \omega_N - m(P - P_{ref}) \tag{3}$$

$$V = V_N - n(Q - Q_{ref}) \tag{4}$$

The swing equations are expressed as

$$J\omega\frac{d(\omega-\omega_N)}{dt} = P_{ref} - P_e - D(\omega-\omega_N) + \frac{1}{m}(\omega_N - \omega) \tag{5}$$

C. CHARGE–DISCHARGE BATTERY CONTROLLER

Fig. 9 presents the battery control for two cases: charge and discharge. The voltage source of the bidirectional converter is the output of the boost converter. The battery parameters are shown in Table 2.

V_B represents the battery voltage, and I_B represents the battery current. The reference charge and discharge current are $I_{B\text{-ref. cha.}}$ and $I_{B\text{-ref.dis.}}$, respectively. The S_{-P} is the pulse for the positive switch part of the bidirectional converter, and S_{-N} is the pulse for the negative side.

TABLE 3. The VSG parameters.

Quantity	Value
AC voltage	220 V
Inverter switching frequency	5 kHz
P_{ref}	2 kW
Q_{ref}	0.5 kvar
L_f	8 mH
C_f	10 µF
R_f	0.01 Ω

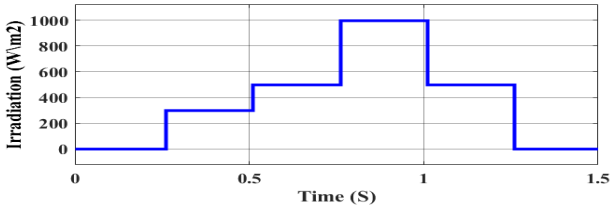

FIGURE 10. The irradiation scheme.

IV. RESULTS

Simulation studies validated the process model and method presented in Fig. 1. Three scenarios based on the model described in Fig. 1 were simulated to investigate the VSG controller performance. The parameters in Table 3 are used.

The selection range of Table 3 parameters used values available in the lab to conform with the experimental part of the work.

A. SCENARIO A: DIFFERENT IRRADIANCE VALUES

Fig. 10 shows the irradiation applied to the PV. The curve, as shown in the figure, contains various irradiations with a maximum value of 1000 W/m^2. The PV voltage and first-stage voltage followed the change in radiation, as shown in Fig. 11 (a) and Fig. 11(b), respectively. At the first stage, the PV rose to 130 V and boosted voltage to 500 V. This is caused by the nature of the MPPT method in PV, and it provided details for the control behavior.

The current results of the PV array and boost converter output are given in Fig. 12(a) and Fig. 12 (b), respectively. The PV current is approximately 50 A, while the boost converter current decreases to 10 A. This decrease depends on the design of the boost converter. Fig. 13 shows the results of the inverter voltage and current for the output load. The inverter side is connected with the load and the output power waveforms shown in Fig. 14.

B. SCENARIO B: IRRADIANCE CURVE VALUES

Fig. 15 depicts the irradiation curve. The curve also contains various values, as seen in the diagram. The voltage response

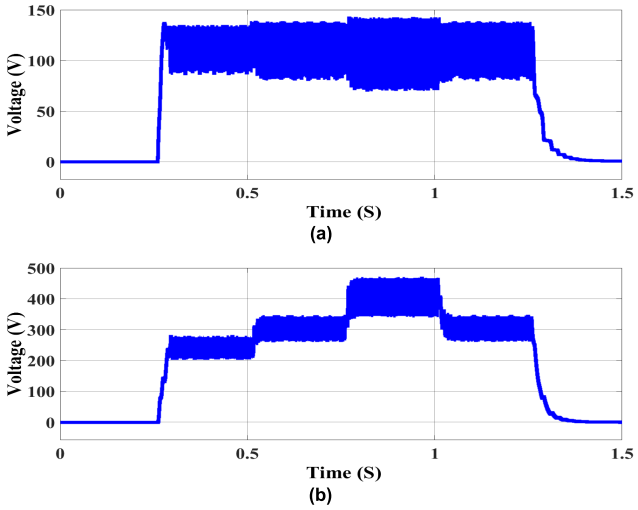

FIGURE 11. Voltage results: (a) PV voltage; (b) boost converter voltage.

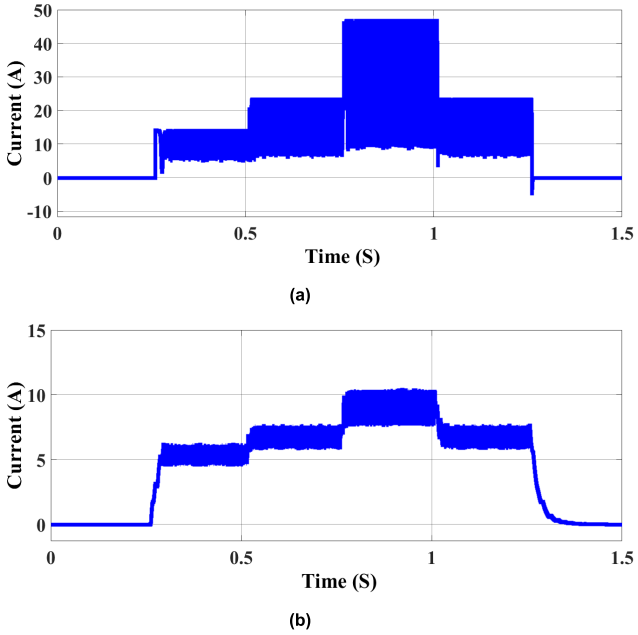

FIGURE 12. Current waveforms: (a) PV current; (b) boost converter output current.

to the new irradiation curve change was plotted for PV voltage and output voltage of the DC-DC stage, as shown in Fig. 16. As seen in Fig. 17, the MPPT tracks the maximum power point (MPP) with 99% efficiency from the PV panel. The control method applied in [16] has been compared with this paper in terms of efficiency. The PV power result is simulated in [16], and the MPPT algorithm tracks a 98% efficiency applied method based on model predictive control. In this paper, the VSG control method was used, as it provides a higher efficiency rate. The advantages of this control method are used for the inverter to behave as a synchronous generator, used for operating inverters in parallel, and for the stability of

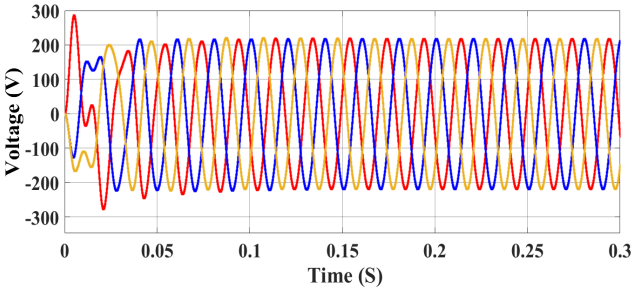

(a)

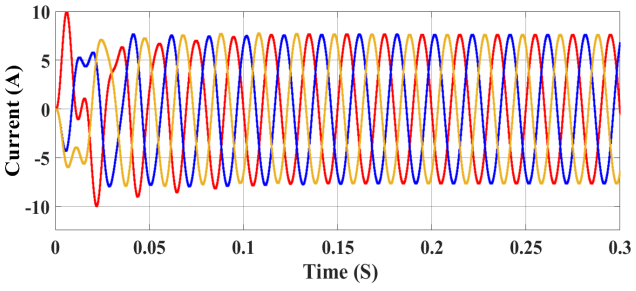

(b)

FIGURE 13. The output load: (a) voltage; (b) current.

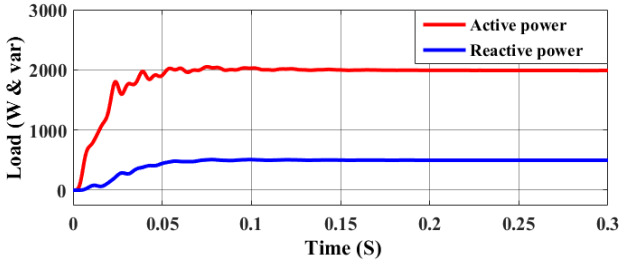

FIGURE 14. The load active and reactive power.

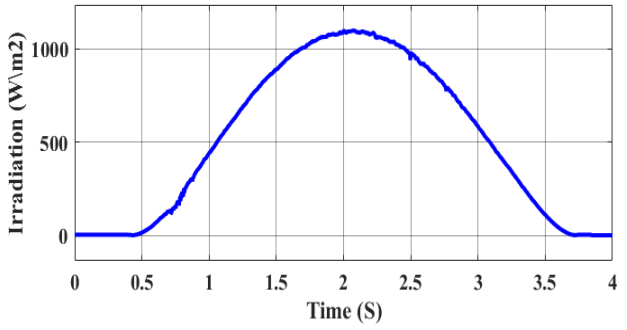

FIGURE 15. The irradiation curve scheme.

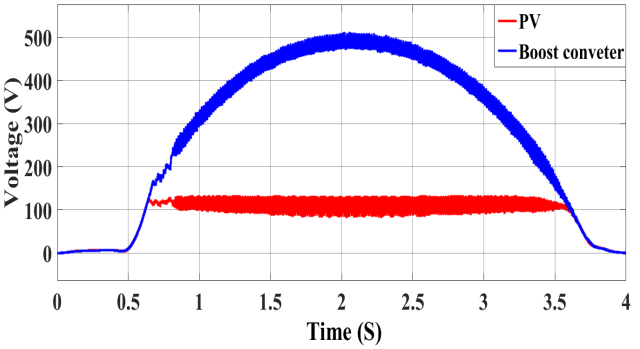

FIGURE 16. The PV and boost converter voltage.

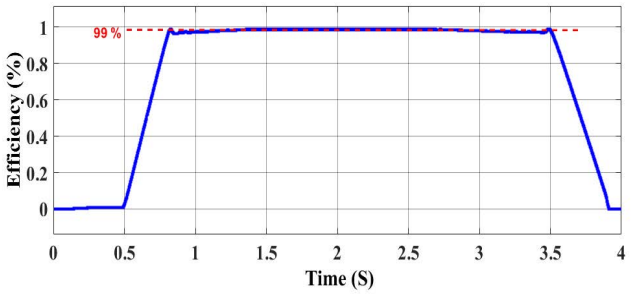

FIGURE 17. The MPPT efficiency.

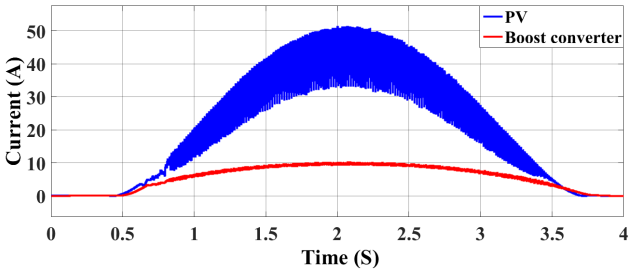

FIGURE 18. The PV and boost converter current.

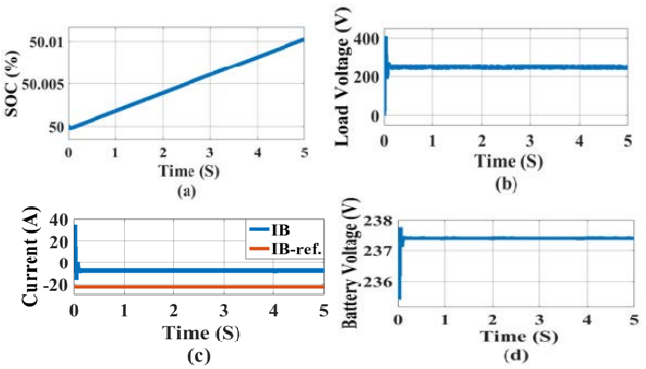

FIGURE 19. Battery charge mode: (a) the state of charge; (b) load voltage; (c) reference and battery current; (d) battery voltage.

a weak power grid or islanding mode [17]–[20]. Fig. 18 shows the PV array and boost converter current.

C. SCENARIO C: BATTERY CHARGE AND DISCHARGE

In the two cases of charging and discharging, a battery bidirectional converter is used. The voltage source "boost converter output" enabled the battery to charge with the load supplied from the source voltage in charging mode, as shown in Fig. 19. The state-of-charge (SOC) is 50%, as shown in Fig. 19 (a). The load voltage is 220 V, and the battery

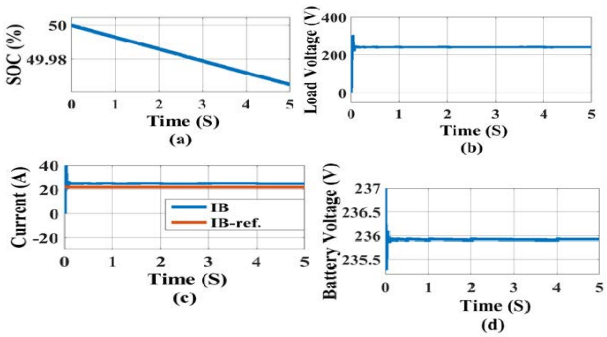

FIGURE 20. Battery discharge mode: (a) the state of charge; (b) load voltage; (c) reference and battery current; (d) battery voltage.

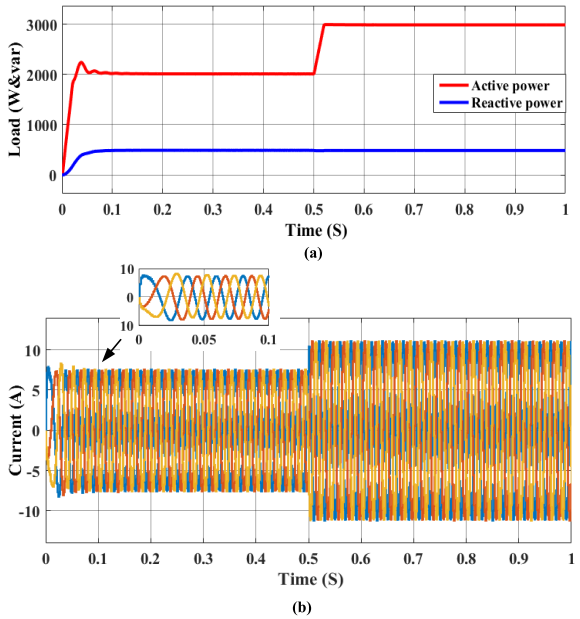

FIGURE 21. Response to output load changes: (a) active and reactive power; (b) output current.

TABLE 4. The experimental VSG parameters.

Quantity	Value
AC voltage	220 V
P_{ref}	1.2 kW
Q_{ref}	0 kvar
L_f	8 mH
C_f	10 µF
R_L	100 Ω

voltage is charged with a value of 237.5 volts, as presented in Fig. 19 (b) and Fig. 19(d). Fig. 19(c) presents the battery reference current IB on this mode selected as −20 A, and the battery charging current is −10 A.

In the discharging mode, the source voltage is disabled, and the battery supplies the load. Fig. 20 shows the discharge operation. The reference current is 20 A, and the battery is discharged with 236 V and 21 A. The battery is connected in

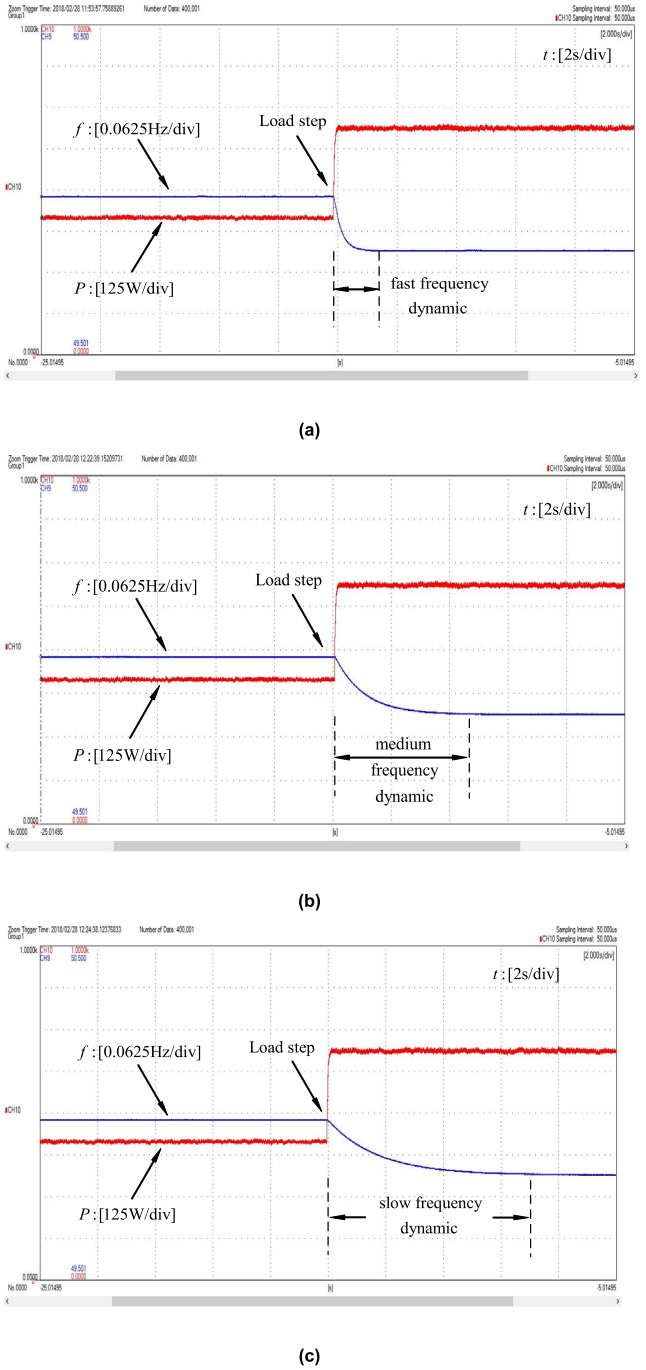

FIGURE 22. Change in virtual inertia, J: (a) J = 0.2 kg.m2; (b) J = 0.8 kg.m2; (c) J = 1.4 kg.m2.

scenarios A and B. The battery status results at scenarios A and B have the same results as in scenario C.

D. SCENARIO D: THE BEHAVIOR OF THE SYSTEM IN RESPONSE TO "LOAD CHANGES"

This scenario mainly discusses the response to load changes to verify the VSG control technology that has been successfully deployed to be applied effectively for this system. If the time (S) axis in Fig. 21 (a) is observed, it is

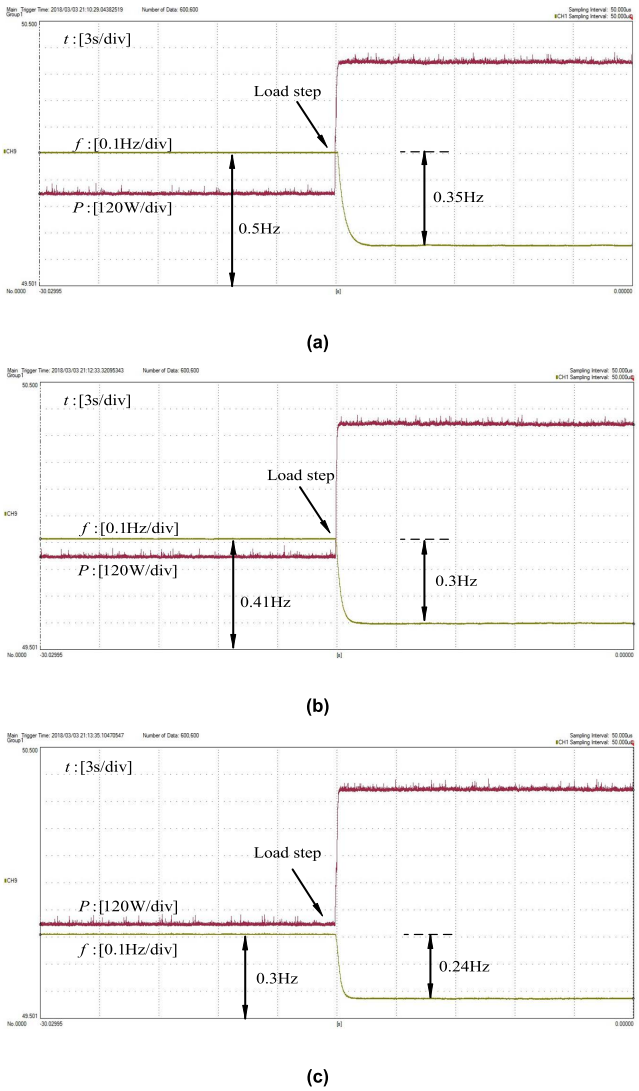

FIGURE 23. Change in droop coefficient, m: (a) m = 0.0014; (b) m = 0.0016; (c) m = 0.002.

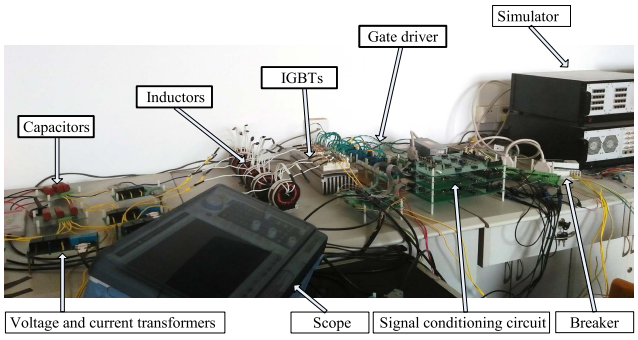

FIGURE 24. The system implementation.

noted that at the 0.5 s mark, another load of 1 kW was added spontaneously and suddenly to evaluate the system performance. As seen, a smooth response has been achieved for active power, as shown in Fig. 21(a). Load output current responses under the load changes are depicted in Fig. 21(b), which proves the effectiveness of the controller.

V. EXPERIMENT OF VSG CONTROL RESULTS

This experiment was carried out via a system containing a single inverter, a load in island mode, and its VSG control circuit. The experimental parameters are given in Table 4.

A. SCENARIO A: CHANGE IN VIRTUAL INERTIA, J

This experiment was carried out for different virtual inertia J = 0.2, 0.8, and 1.4, with the load stepped from 100 Ω to 150 Ω. The results are shown in Fig. 22. Every waveform is the VSG frequency or the active load power. As seen, any increase in the virtual inertia considerably improves the frequency dynamics.

B. SCENARIO B: CHANGE IN DROOP COEFFICIENT, m

In this experiment, VSG was subjected to a sudden increase in load by 50 Ω/70 mH. The simulation was repeated with different values of m, given m = 0.0014, 0.0016, 0.002 to make clear the effect of the droop coefficient. Fig. 23 shows the results. The system implemented is shown in Fig. 24.

VI. CONCLUSION

The paper proposes two-stage converter PV systems, including a battery unit. MPPT algorithms and VSG control used in the proposed control strategy. Additionally, a bidirectional converter control is presented. The combined control provided successful tracking under various irradiation scenarios thanks to the proposed method's quick and responsive control capability. In addition to the combined control performance tests and the favorable effects on the whole system, it is seen from the bidirectional battery method that the control of battery modes also has superior control capacity. The MPPT control was subjected to efficiency analysis. The MPPT system has a 99% control efficiency. The experiment proved that the inertia increase greatly improves the frequency dynamics. This means that VSG can truly and very precisely model a synchronous generator. Therefore, it is considered a good controller for this system.

REFERENCES

[1] P. S. Shenoy, K. A. Kim, B. B. Johnson, and P. T. Krein, "Differential power processing for increased energy production and reliability of photovoltaic systems," *IEEE Trans. Power Electron.*, vol. 28, no. 6, pp. 2968–2979, Jun. 2013, doi: 10.1109/TPEL.2012.2211082.

[2] X. Lu, K. Sun, J. M. Guerrero, J. C. Vasquez, and L. Huang, "State-of-charge balance using adaptive droop control for distributed energy storage systems in DC microgrid applications," *IEEE Trans. Ind. Electron.*, vol. 61, no. 6, pp. 2804–2815, Jun. 2014, doi: 10.1109/TIE.2013.2279374.

[3] M. Sechilariu, B. Wang, and F. Locment, "Building integrated photovoltaic system with energy storage and smart grid communication," *IEEE Trans. Ind. Electron.*, vol. 60, no. 4, pp. 1607–1618, Apr. 2013, doi: 10.1109/TIE.2012.2222852.

[4] Z. Liang, R. Guo, J. Li, and A. Q. Huang, "A high-efficiency PV module-integrated DC/DC converter for PV energy harvest in FREEDM systems," *IEEE Trans. Power Electron.*, vol. 26, no. 3, pp. 897–909, Mar. 2011, doi: 10.1109/TPEL.2011.2107581.

[5] M. Shayestegan, "Overview of grid-connected two-stage transformerless inverter design," *J. Mod. Power Syst. Clean Energy*, vol. 6, no. 4, pp. 642–655, Jan. 2018, doi: 10.1007/s40565-017-0367-z.

[6] S. Wei, F. He, L. Yuan, Z. Zhao, T. Lu, and J. Ma, "Design and implementation of high efficient two-stage three-phase/level isolated PV converter," in *Proc. 18th Int. Conf. Electr. Mach. Syst. (ICEMS)*, Pattaya, Thailand, Oct. 2015, pp. 1649–1654.
[7] A. Sangwongwanich and F. Blaabjerg, "Mitigation of interharmonics in PV systems with maximum power point tracking modification," *IEEE Trans. Power Electron.*, vol. 34, no. 9, pp. 8279–8282, Sep. 2019, doi: 10.1109/TPEL.2019.2902880.
[8] R. Boukenoui, M. Ghanes, J.-P. Barbot, R. Bradai, A. Mellit, and H. Salhi, "Experimental assessment of maximum power point tracking methods for photovoltaic systems," *Energy*, vol. 132, pp. 324–340, Aug. 2017, doi: 10.1016/j.energy.2017.05.087.
[9] N. A. Ninad and L. A. C. Lopes, "Operation of single-phase grid-connected inverters with large DC bus voltage ripple," in *Proc. IEEE Canada Electr. Power Conf.*, Montreal, QC, Canada, Oct. 2007, pp. 172–176, doi: 10.1109/EPC.2007.4520325.
[10] S. B. Kjaer, J. K. Pedersen, and F. Blaabjerg, "A review of single-phase grid-connected inverters for photovoltaic modules," *IEEE Trans. Ind. Appl.*, vol. 41, no. 5, pp. 1292–1306, Sep. 2005, doi: 10.1109/TIA.2005.853371.
[11] R. Wai and W. Wang, "Grid-connected photovoltaic generation system," *IEEE Trans. Circuits Syst.*, vol. 55, no. 3, pp. 953–963, Apr. 2008, doi: 10.1109/TCSI.2008.919744.
[12] D. Debnath and K. Chatterjee, "Transformer coupled multi-input two stage standalone solar photovoltaic scheme for rural areas," in *Proc. 39th Annu. Conf. IEEE Ind. Electron. Soc. (IECON)*, Vienna, Austria, Nov. 2013, pp. 7028–7033, doi: 10.1109/IECON.2013.6700298.
[13] T.-F. Wu, "Power loss comparison of Single- and two-stage grid-connected photovoltaic systems," *J. Electr. Electron. Eng.*, vol. 26, no. 2, pp. 11–19, Jun. 2014, doi: 10.1109/TEC.2011.2123897.
[14] N. H. Selman and J. R. Mahmood, "Design and simulation of two stages single phase PV inverter operating in standalone mode without batteries," *Int. J. Eng. Trends Technol.*, vol. 37, no. 2, pp. 102–109, Jul. 2016, doi: 10.14445/22315381/IJETT-V37P217.
[15] Y. Amara, R. Boukenoui, R. Bradai, and H. Salhi, "Design and control of two-stage standalone photovoltaic generation system," in *Proc. Int. Conf. Commun. Electr. Eng. (ICCEE)*, El Oued, Algeria, Dec. 2018, pp. 1–5, doi: 10.1109/CCEE.2018.8634511.
[16] N. Guler and E. Irmak, "MPPT based model predictive control of grid connected inverter for PV systems," in *Proc. 8th Int. Conf. Renew. Energy Res. Appl. (ICRERA)*, Brasov, Romania, Nov. 2019, pp. 982–986.
[17] J. Alipoor, Y. Miura, and T. Ise, "Distributed generation grid integration using virtual synchronous generator with adoptive virtual inertia," in *Proc. IEEE Energy Convers. Congr. Expo. (ECCE)*, Denver, CO, USA, Sep. 2013, pp. 4546–4552.
[18] J. Alipoor, Y. Miura, and T. Ise, "Power system stabilization using virtual synchronous generator with alternating moment of inertia," *IEEE J. Emerg. Sel. Topics Power Electron.*, vol. 3, no. 2, pp. 451–458, Jun. 2015, doi: 10.1109/JESTPE.2014.2362530.
[19] K. Sakimoto, Y. Miura, and T. Ise, "Stabilization of a power system with a distributed generator by a virtual synchronous generator function," in *Proc. 8th Int. Conf. Power Electron. (ECCE Asia)*, Jeju, South Korea, May/Jun. 2011, pp. 1498–1505.
[20] S. Rubino, A. Mazza, G. Chicco, and M. Pastorelli, "Advanced control of inverter-interfaced generation behaving as a virtual synchronous generator," in *Proc. IEEE Eindhoven PowerTech*, Eindhoven, The Netherlands, Jun./Jul. 2015, pp. 1–6.

HASHIM HASABELRASUL received the Ph.D. degree in electrical engineering from the School of Electrical and Electronic Engineering, North China Electric Power University, China, in 2019. He is currently a Postdoctoral Researcher with the School of Mechanical and Electrical Engineering, Hebei Agricultural University, China. His current research interests include power electronics applications in power systems, storage systems, microgrids, and virtual synchronous machines.

ZHENJIANG CAI received the Ph.D. degree in detection technology and automation equipment from the Beijing University of Technology, China, in 2005. He is currently a Professor and the Doctoral Supervisor at the School of Mechanical and Electrical Engineering, Hebei Agricultural University, China. His main research interests include intelligent detection and control, digital image recognition, and measurement and control devices.

LEI SUN received the M.S. degree in electrical engineering from North China Electric Power University, China, in 2015. He is currently pursuing the Ph.D. degree in agricultural electrification with the School of Mechanical and Electrical Engineering, Hebei Agricultural University, China. He is a Master's Tutor at Hebei Agricultural University. His research interests include machine vision, deep learning, and detection technology.

XUESONG SUO received the master's degree in agricultural mechanization engineering from the School of Mechanical and Electrical Engineering, Hebei Agricultural University, China, in 2003. He is currently a Professor and the Master's Tutor at Hebei Agricultural University. His research interests include agricultural engineering and smart agriculture.

IMAD MATRAJI received the master's degree in engineering and management of industrial systems and the Ph.D. degree in automatic control systems from the University of Technology of Belfort-Montbeliard (UTBM), Belfort, France, in 2009 and 2013, respectively. In 2017, he joined Great Wall Motor as the Chief Engineer for fuel cell control systems. His research interests include PEM fuel cell control systems for automotive application, renewable energy management and power systems, and robotics.